# On a Three-Layer Approximation of Two-Layer Shallow Water Equations

Alina Chertock*, Alexander Kurganov†, Zhuolin Qu‡and Tong Wu§

**Abstract**

Two-layer shallow water equations describe flows that consist of two layers of inviscid fluid of different, constant densities flowing over bottom topography. Unlike the singe-layer shallow water system, the two-layer one is only conditionally hyperbolic: It loses its hyperbolicity because of the momentum exchange terms between the layers and as the results its solutions may develop instabilities. We study a three-layer approximation of the two-layer shallow water equations by introducing an intermediate layer of a small depth. We examine the hyperbolicity range of the three-layer model and demonstrate that while it still may lose hyperbolicity, in some cases, the three-layer approximation may improve stability properties of the two-layer shallow water system.

## 1 Introduction

Shallow water models are widely used as a mathematical framework to study water flows in rivers and coastal areas as well as to investigate a variety of phenomena in atmospheric sciences and oceanography. The basic feature of shallow water flows is that the vertical effect can be neglected compared with the horizontal one with a good approximation. This allows a considerable simplification in the mathematical formulation by replacing the vertical momentum equation by the hydrostatic pressure distribution. As a result, such flows are usually described by the shallow water equations. The simplest, yet commonly used, shallow water model is the Saint-Venant system [11].

Layered shallow water equations describe the behaviour of several superposed layers of inviscid fluid of different, constant densities flowing over bottom topography, as illustrated in Figure 1.1, and are derived by depth averaging the incompressible Navier-Stokes equations with the hydrostatic assumption within each layer. For instance, the following one-dimensional (1-D) two-layer shallow water model describes a flow that consists of layers of heights $h_1$ (upper layer) and $h_2$ (lower layer) at position $x$ at time $t$ with the corresponding constant densities $\rho_1 < \rho_2$, velocities

*Department of Mathematics, North Carolina State University, Raleigh, NC 27695, USA; chertock@math.ncsu.edu

†Mathematics Department, Tulane University, New Orleans, LA 70118, USA; kurganov@math.tulane.edu

‡Mathematics Department, Tulane University, New Orleans, LA 70118, USA; zqu1@tulane.edu

§Mathematics Department, Tulane University, New Orleans, LA 70118, USA; twu2@tulane.edu

$u_1$ and $u_2$, and discharges $q_1 := h_1u_1$ and $q_2 := h_2u_2$:

$$\begin{cases} (h_1)_t + (q_1)_x = 0, \\ (q_1)_t + \left(h_1u_1^2 + \dfrac{g}{2}h_1^2\right)_x = -gh_1B_x - gh_1(h_2)_x, \\ (h_2)_t + (q_2)_x = 0, \\ (q_2)_t + \left(h_2u_2^2 + \dfrac{g}{2}h_2^2\right)_x = -gh_2B_x - grh_2(h_1)_x. \end{cases} \tag{1.1}$$

Here, $B(x)$ is a function describing the bottom topography, $r = \frac{\rho_1}{\rho_2}$ is the ratio of the densities, which is typically $r \sim 1$, and $g$ is the gravitational constant.

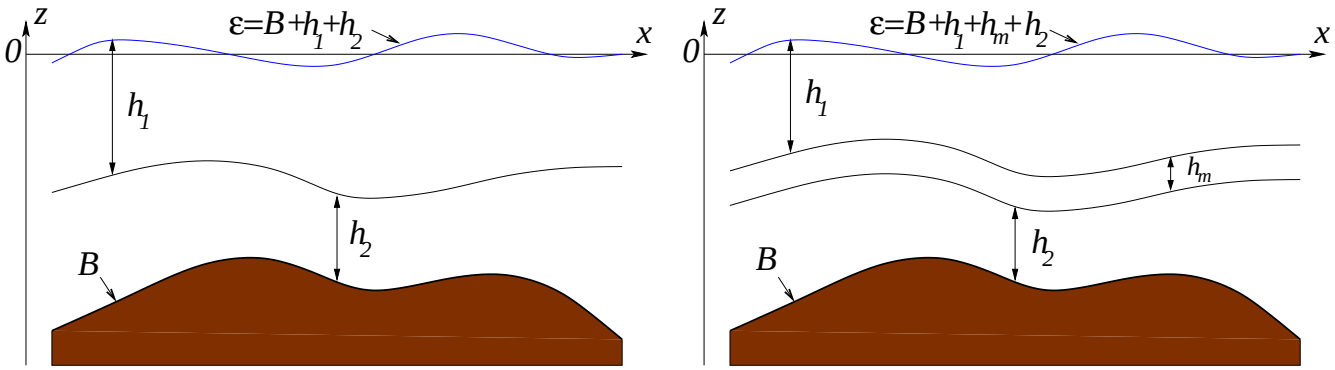


Figure 1.1: Two-layer (left) and three-layer (right) shallow water setup.

The system (1.1) consists of four equations: The first and third of which indicate the conservation of mass, and the second and fourth equations state the momentum balance for each layer. One of the key challenges in solving the system (1.1) numerically is that it is only conditionally hyperbolic which may lead to significant instabilities. Specifically speaking, the hyperbolic region of the system (1.1) mainly depends on the difference between the velocities of the two layers: When $|u_1-u_2|$ is large, the system is not hyperbolic and one may expect appearance of Kelvin-Helmholtz instabilities. Another numerical challenge is related to the presence of nonconservative momentum exchange terms on the right-hand side (RHS) of (1.1). Even though the analytic theory of nonconservative hyperbolic system has been developed (see, e.g., [10]), designing a numerical scheme whose solution is guaranteed to converge to the unique physically relevant solution is still an open problem. A theoretical framework for designing converging numerical method was presented in [24], and a class of path-conservative schemes was developed afterwards in [7, 9, 22]. However, as it has been recently demonstrated in [2], convergence of path-conservative schemes has still not been rigorously established. In [17], an alternative approach was proposed. The system (1.1) was rewritten in a different form, which is equivalent to (1.1) for smooth solutions:

$$\begin{cases} (h_1)_t + (q_1)_x = 0, \\ (q_1)_t + \left(\dfrac{q_1^2}{h_1} + g\varepsilon h_1\right)_x = g\varepsilon(h_1)_x, \\ w_t + (q_2)_x = 0, \\ (q_2)_t + \left(\dfrac{q_2^2}{w-B} + \dfrac{g}{2}w^2 - \dfrac{g}{2}rh_1^2 - gB(rh_1+w)\right)_x = -g(rh_1+w)B_x - gr\varepsilon(h_1)_x, \end{cases} \tag{1.2}$$

where $w := h_2 + B$ and $\varepsilon := h_1 + h_2 + B$. The main advantage of the rewritten system (1.2) over the original one (1.1) is that the coefficients of the nonconservative product terms on the RHS of (1.2) are now proportional to the water surface variable $\varepsilon$, which is typically small in all realistic settings provided that the reference level in the vertical direction $z$ is selected to be 0 (see Figure 1.1). This is obviously true in all of the oceanographic applications, in which the magnitude of surface waves is much smaller than the depth of the ocean. In [17], the system (1.2) was numerically solved using a well-balanced, positivity-preserving central-upwind scheme, which was originally developed for hyperbolic systems of conservation laws [14,15,18,19] and then extended and applied to hyperbolic systems of balance laws arising in modeling shallow water flows, see [13,16,17]. For several other numerical methods for multilayer shallow water equations we refer the reader, e.g., to [1,3–5].

One of the reasons the system (1.1) (and also its rewritten version (1.2)) is only conditionally hyperbolic is that it is derived using a non-mixing assumption. In this paper, we study a three-layer approximation of the two-layer system (1.1), which is obtained by introducing an intermediate layer of a (small) depth $h_m$. Our main goal is to study whether having an additional, "buffer" layer would help to regain hyperbolicity in cases it is lost since the new layer is expected to contain all possible turbulence and mixing without substantially affecting the horizontal velocities of the other layers. We test a simple strategy of adding a "buffer" layer at the initial time moment and see how it develops in time. A more sophisticated adaptive procedure was proposed in [6], where the width of the intermediate layer was modified dynamically to make sure that a meaningful "buffer" zone is always present between the upper and lower layers. Although the three-layer system may still lose hyperbolicity as it demonstrated in §5 below, we show that the proposed three-layer approximation may improve stability properties of the shallow water system in some cases. At the same time, the loss of hyperbolicity seems to be a generic feature of the studied three-layer system even though its hyperbolicity range may be much larger than the one of the corresponding two-layer system, especially when the width of the "buffer" layer is large. As we demonstrate in one of our numerical experiments, it may happen that the solution of the three-layer system develops more severe oscillations than the original two-layer system. This suggests that a further study is required to better understand the extent of applicability of the studied three-layer system.

The paper is organized as follows. In §2, we present the three-layer approximation of the two-layer shallow water system and discuss the strategy for choosing the intermediate layer. In §3, we derive the central-upwind scheme for the three-layer system. Finally, §4 and §5 contain numerical examples and analysis of the hyperbolicity properties of the three-layer shallow water equations.

## 2 The Three-Layer Shallow Water System

In this section, we introduce a three-layer shallow water system by adding an intermediate layer with the depth $h_m$, velocity $u_m$ and discharge $q_m$ to system (1.1). The new system reads, (for the form of a general multilayer system we refer the reader to [3])

$$\begin{cases} (h_1)_t + (q_1)_x = 0,\\ (q_1)_t + \left(h_1u_1^2 + \dfrac{g}{2}h_1^2\right)_x = -gh_1B_x - gh_1(h_m + h_2)_x,\\ (h_m)_t + (q_m)_x = 0,\\ (q_m)_t + \left(h_mu_m^2 + \dfrac{g}{2}h_m^2\right)_x = -gh_mB_x - g\dfrac{2r}{1+r}h_m(h_1)_x - gh_m(h_2)_x,\\ (h_2)_t + (q_2)_x = 0,\\ (q_2)_t + \left(h_2u_2^2 + \dfrac{g}{2}h_2^2\right)_x = -gh_2B_x - g\dfrac{1+r}{2}h_2(h_m)_x - grh_2(h_1)_x. \end{cases} \tag{2.1}$$

To apply the central-upwind scheme to this system, we follow the approach in [17] and rewrite it as follows:

$$\begin{cases} (h_1)_t + (q_1)_x = 0,\\ (q_1)_t + \left(\dfrac{q_1^2}{h_1} + g\varepsilon h_1\right)_x = g\varepsilon(h_1)_x,\\ (h_m)_t + (q_m)_x = 0,\\ (q_m)_t + \left(\dfrac{q_m^2}{h_m} + g\varepsilon h_m\right)_x = g\varepsilon(h_m)_x + g\dfrac{1-r}{1+r}h_m(h_1)_x,\\ w_t + (q_2)_x = 0,\\ (q_2)_t + \left(\dfrac{q_2^2}{w-B} + \dfrac{g}{2}w^2 - \dfrac{g}{2}rh_1^2 - gB(rh_1+w) - g\dfrac{1+r}{2}h_m(h_1+B) - g\dfrac{1+r}{4}h_m^2\right)_x\\ \qquad = -g\left(rh_1 + w + \dfrac{1+r}{2}h_m\right)B_x - g\varepsilon\left(r(h_1)_x + \dfrac{1+r}{2}(h_m)_x\right) - g\dfrac{1-r}{2}h_m(h_1)_x. \end{cases} \tag{2.2}$$

As in the two-layer system (1.2), we have introduced the new equilibrium variables $w := h_2 + B$ and the water surface $\varepsilon := h_1 + h_m + h_2 + B$. Notice that the formula for $\varepsilon$ is now different from the one used in (1.2) since we have one extra layer to be added. At the same time, we set up the scales at the vertical $z$-axis so that the reference surface level is 0 (see Figure 1.1, right) as it was done in the two-layer case schematically presented in Figure 1.1, left.

The new system is preferable for numerical computation thanks for the following two reasons:

(i) Since the system (2.2) is written in terms of equilibrium variables, the "lake at rest" steady-state solution takes a particularly nice form:

$$h_1 \equiv \text{const}, \quad h_m \equiv \text{const}, \quad w \equiv \text{const}, \quad u_1 \equiv u_2 \equiv u_m \equiv 0. \tag{2.3}$$

Thus, the reformulated system makes it simpler to derive a well-balanced scheme for the three-layer shallow water equations;

(ii) The coefficients in the nonconservative terms on the RHS of (2.2) are proportional to either $\varepsilon$ or $(1-r)h_m$. Note that $\varepsilon$ vanishes at the "lake at rest" steady states, and, what is even more important, in most oceanographic application remains very small. We also do not expect the depth of the intermediate layer to become large in any realistic scenario, which means that $(1-r)h_m$ is also expected to remain small. Smallness of $\varepsilon$ and $(1-r)h_m$ is expected to make the computed results to be practically independent of the way the nonconservative terms are discretized as it was the case in [17].

**Remark 2.1** Notice that if one sets $h_m = q_m \equiv 0$, the three-layer system (2.2) reduces to the two-layer system (1.2).

# 3 Central-Upwind Scheme for the Three-Layer System

In this section, we describe a second-order well-balanced, positivity preserving central-upwind scheme for the three-layer shallow water system (2.2), which we rewrite in the vector form as

$$\mathbf{U}_t + \mathbf{F}(\mathbf{U}, B)_x = \mathbf{S}(\mathbf{U}, B) + \mathbf{N}(\mathbf{U}, B), \tag{3.1}$$

where the unknown function $\mathbf{U}$, flux $\mathbf{F}$, geometric source term $\mathbf{S}$ and nonconservative product term $\mathbf{N}$ are given by the following formulae:

$$\begin{aligned}
\mathbf{U} &:= (h_1, q_1, h_m, q_m, w, q_2)^T,\\
\mathbf{F}(\mathbf{U}, B) &:= \Bigg(q_1, \frac{q_1^2}{h_1} + g\varepsilon h_1, q_m, \frac{q_m^2}{h_m} + g\varepsilon h_m, q_2,\\
&\qquad \frac{q_2^2}{w-B} + \frac{g}{2}w^2 - \frac{g}{2}rh_1^2 - gB(rh_1 + w) - g\frac{1+r}{2}h_m(h_1 + B) - g\frac{1+r}{4}h_m^2\Bigg)^T,\\
\mathbf{S}(\mathbf{U}, B) &:= \Bigg(0, 0, 0, 0, 0, -g\Big(rh_1 + w + \frac{1+r}{2}h_m\Big)B_x\Bigg)^T,\\
\mathbf{N}(\mathbf{U}, B) &:= \Bigg(0, g\varepsilon(h_1)_x, 0, g\varepsilon(h_m)_x + g\frac{1-r}{1+r}h_m(h_1)_x,\\
&\qquad 0, -gr\varepsilon(h_1)_x - g\frac{1+r}{2}\Big(\varepsilon(h_m)_x + \frac{1-r}{1+r}h_m(h_1)_x\Big)\Bigg)^T.
\end{aligned} \tag{3.2}$$

We divide the computational domain into the cells $C_j = [x_{j-\frac{1}{2}}, x_{j+\frac{1}{2}}]$, which for simplicity are assumed to be uniform so that $x_{j+\frac{1}{2}} - x_{j-\frac{1}{2}} = \Delta x$ and $x_j = j\Delta x$ for all $j$. We denote by

$$\overline{\mathbf{U}}_j(t) = \frac{1}{\Delta x}\int\limits_{C_j} \mathbf{U}(x,t)\,dx$$

the computed cell averages of $\mathbf{U}$, which we assume to be available at time t. Using the notations introduced in (3.2), a semi-discretization of (3.1) can be written as the following system of ODEs:

$$\frac{d}{dt}\overline{\mathbf{U}}_j(t) = -\frac{\mathbf{H}_{j+\frac{1}{2}}(t) - \mathbf{H}_{j-\frac{1}{2}}(t)}{\Delta x} + \overline{\mathbf{S}}_j(t) + \overline{\mathbf{N}}_j(t), \tag{3.3}$$

where $\mathbf{H}_{j+\frac{1}{2}}$ are numerical fluxes, and $\overline{\mathbf{S}}_j$ and $\overline{\mathbf{N}}_j$ are discretizations of the geometric source and nonconservative product terms, respectively:

$$\overline{\mathbf{S}}_j(t) \approx \frac{1}{\Delta x}\int\limits_{C_j} \mathbf{S}(\mathbf{U}(x,t), B(x))\,dx, \quad \overline{\mathbf{N}}_j(t) \approx \frac{1}{\Delta x}\int\limits_{C_j} \mathbf{N}(\mathbf{U}(x,t), B(x))\,dx. \tag{3.4}$$

We use the central-upwind numerical fluxes derived in [15] (see also [13, 16, 17, 19]):

$$\mathbf{H}_{j+\frac{1}{2}} = \frac{a^+_{j+\frac{1}{2}}\mathbf{F}(\mathbf{U}^-_{j+\frac{1}{2}}, B_{j+\frac{1}{2}}) - a^-_{j+\frac{1}{2}}\mathbf{F}(\mathbf{U}^+_{j+\frac{1}{2}}, B_{j+\frac{1}{2}})}{a^+_{j+\frac{1}{2}} - a^-_{j+\frac{1}{2}}} + \frac{a^+_{j+\frac{1}{2}}a^-_{j+\frac{1}{2}}}{a^+_{j+\frac{1}{2}} - a^-_{j+\frac{1}{2}}}\Big[\mathbf{U}^+_{j+\frac{1}{2}} - \mathbf{U}^-_{j+\frac{1}{2}}\Big]. \tag{3.5}$$

Here, $B_{j+\frac12} := B(x_{j+\frac12})$ (or $B_{j+\frac12} := \frac12\big(B(x_{j+\frac12}+0)+B(x_{j+\frac12}-0)\big)$ in the case the bottom topography function $B$ is discontinuous at $x = x_{j+\frac12}$), $\mathbf{U}^{\pm}_{j+\frac12}$ are the right/left point values at $x = x_{j+\frac12}$ of the conservative piecewise linear reconstruction

$$\widetilde{\mathbf{U}}(x) := \overline{\mathbf{U}}_j + (\mathbf{U}_x)_j\,(x-x_j)\,, \quad x \in C_j, \tag{3.6}$$

so that

$$\mathbf{U}^{-}_{j+\frac12} := \widetilde{\mathbf{U}}\left(x_{j+\frac12}-0\right) = \overline{\mathbf{U}}_j + \frac{\Delta x}{2}\,(\mathbf{U}_x)_j\,, \quad \mathbf{U}^{+}_{j+\frac12} := \widetilde{\mathbf{U}}\left(x_{j+\frac12}+0\right) = \overline{\mathbf{U}}_{j+1} - \frac{\Delta x}{2}\,(\mathbf{U}_x)_j\,. \tag{3.7}$$

The numerical derivatives $(\mathbf{U}_x)_j$ are at least first-order accurate approximations of $\mathbf{U}_x(x_j,t)$, computed using a nonlinear limiter needed to ensure a non-oscillatory nature of the reconstruction (3.6). In our numerical computations, we have used the generalized minmod limiter:

$$(\mathbf{U}_x)_j = \text{minmod}\left(\theta\frac{\overline{\mathbf{U}}_j-\overline{\mathbf{U}}_{j-1}}{\Delta x},\ \frac{\overline{\mathbf{U}}_{j+1}-\overline{\mathbf{U}}_{j-1}}{2\Delta x},\ \theta\frac{\overline{\mathbf{U}}_{j+1}-\overline{\mathbf{U}}_j}{\Delta x}\right), \quad \theta\in[1,2], \tag{3.8}$$

where the minmod function, defined as

$$\text{minmod}(z_1,z_2,\ldots) := \begin{cases} \min\limits_j\{z_j\}, & \text{if } \ z_j>0\ \forall j,\\ \max\limits_j\{z_j\}, & \text{if } \ z_j<0\ \forall j,\\ 0, & \text{otherwise,}\end{cases}$$

is applied in a componentwise manner. The parameter $\theta$ can be used the control the amount of numerical viscosity present in the resulting scheme (see, e.g., [20, 23] for more details). In our numerical experiments, we use $\theta = 1$, which corresponds to the most diffusive minmod reconstruction.

The right- and left-sided local speeds $a^{\pm}_{j+\frac12}$ in (3.5) should be obtained as in [13, 15–17] using the smallest and largest eigenvalues of the Jacobian $\frac{\partial\mathbf{F}}{\partial\mathbf{U}}$. However, the Jacobian of the three-layer shallow water system is a $6\times6$ matrix with no analytical expressions for the eigenvalues available. Moreover, even though the upper/lower bounds on the largest/smallest eigenvalues of this matrix can be obtained using the Lagrange theorem (see, e.g., [21]), as it was done in [17] for the two-layer shallow water system, the resulting bounds are quite cumbersome and computationally expensive. We therefore use the bounds established in [17] for the two-layer system (1.2) (in the calculation of these bounds, we redistribute the intermediate "buffer" layer and replace $h_1$ and $h_2$ in formulae (2.22) and (2.23) from [17] with $h_1+h_m/2$ and $h_2+h_m/2$, respectively). This approach is accurate as long as the velocity of "buffer" layer is in the range of the velocities of the upper and lower layers.

**Remark 3.1** Note that the quantities $\overline{\mathbf{U}}_j$, $\mathbf{U}^{\pm}_{j+\frac12}$, $(\mathbf{U}_x)_j$ and $a^{\pm}_{j+\frac12}$ in (3.5)–(3.8) depend on t, but we simplify the notation by suppressing this dependence.

To ensure nonnegativity of $h_1$, $h_m$ and $h_2$, we follow [16,17] and correct the reconstructed point values of $w$ in each cell $C_j$ according to the following algorithm:

$$\begin{aligned}&\text{If } \ w^{-}_{j+\frac12} < B_{j+\frac12}, \ \text{ then set } \ w^{-}_{j+\frac12} := B_{j+\frac12},\ w^{+}_{j-\frac12} := 2\overline{w}_j - B_{j+\frac12};\\ &\text{If } \ w^{+}_{j-\frac12} < B_{j-\frac12}, \ \text{ then set } \ w^{+}_{j-\frac12} := B_{j-\frac12},\ w^{-}_{j+\frac12} := 2\overline{w}_j - B_{j-\frac12}.\end{aligned}$$

To guarantee that the resulting scheme is well-balanced in the sense that the "lake at rest" steady states (2.3) are preserved, we employ a well-balanced quadrature (developed in [13], see also [16, 17]) and approximate the cell averages of the geometric source term as:

$$\overline{\mathbf{S}}_j(t)=\left(0,0,0,0,0,-g\Big(r(\overline{h_1})_j+\overline{w}_j+\frac{1+r}{2}\,(\overline{h_m})_j\Big)\cdot\frac{B_{j+\frac12}-B_{j-\frac12}}{\Delta x}\right)^T.$$

Finally, we follow [17] and discretize the nonconservative product terms using the same quadrature, which results in

$$\begin{aligned}
\overline{N}_j^{(2)}(t)&=g\overline{\varepsilon}_j\frac{(h_1)^-_{j+\frac12}-(h_1)^+_{j-\frac12}}{\Delta x},\\
\overline{N}_j^{(4)}(t)&=g\overline{\varepsilon}_j\frac{(h_m)^-_{j+\frac12}-(h_m)^+_{j-\frac12}}{\Delta x}+g\frac{1-r}{1+r}(\overline{h_m})_j\frac{(h_1)^-_{j+\frac12}-(h_1)^+_{j-\frac12}}{\Delta x},\\
\overline{N}_j^{(6)}(t)&=-r\overline{N}_j^{(2)}(t)-\frac{1+r}{2}\overline{N}_j^{(4)}(t),
\end{aligned}$$

where $\overline{N}_j^{(2)}$, $\overline{N}_j^{(4)}$ and $\overline{N}_j^{(6)}$ are (nonzero) components of the vector $\overline{\mathbf{N}}_j(t)$ in (3.4), that is, $\overline{\mathbf{N}}_j=\big(0,\overline{N}_j^{(2)},0,\overline{N}_j^{(4)},0,\overline{N}_j^{(6)}\big)^T$.

**Remark 3.2** A fully discrete central-upwind scheme is obtained by applying an appropriate ODE solver to (3.3). In our numerical experiments, we have used the third-order strong stability preserving Runge-Kutta (SSP-RK) method from [12].

**Remark 3.3** As in [16, 17], one can prove that provided the ODE system (3.3) is discretized using an SSP ODE solver and the CFL condition is satisfied with the CFL number equal to 1/2, the presented central-upwind scheme will be positivity preserving in the following sense: If at a certain time level, $(\overline{h_1})_j(t)\ge0$, $(\overline{h_m})_j(t)\ge0$ and $(\overline{h_2})_j(t)\ge0$ for all $j$, then at the next time level $(\overline{h_1})_j(t+\Delta t)\ge0$, $(\overline{h_m})_j(t+\Delta t)\ge0$ and $(\overline{h_2})_j(t+\Delta t)\ge0$ as well. It should be observed that as in [16, 17] we set $(\overline{h_2})_j:=\overline{w}_j-\widetilde{B}(x_j)$ (rather than $\overline{w}_j-B(x_j)$), where $\widetilde{B}$ is a continuous piecewise linear approximant of the bottom topography $B$, namely,

$$\widetilde{B}(x)=B_{j-\frac12}+\Big(B_{j+\frac12}-B_{j-\frac12}\Big)\cdot\frac{x-x_{j-\frac12}}{\Delta x},\quad x\in C_j.$$

**Remark 3.4** Notice that if one sets $(\overline{h_m})_j(0)=(\overline{q_m})_j(0)\equiv0$, the presented central-upwind scheme reduces to the central-upwind scheme from [17] for the two-layer system (1.2).

# 4 Numerical Examples

In this section, we apply the central-upwind scheme developed in §3 to the three-layer shallow water system (2.2). The purpose of the presented numerical experiments is to check whether (and to what extent) the three-layer approximation (2.2) is capable of curing the instabilities that are typically developed in solutions of the two-layer system (1.2) in the nonhyperbolic regime.

In both examples below, we take the gravitational constant $g=10$ and the density ratio $r=0.98$.

**Example 1.** We consider the three-layer shallow water system (2.2) subject to the initial data:

$$h_1(x,0)=\begin{cases}1-\dfrac{1}{2}\widehat{h}_m, & |x|\ge 1,\\ 1-\dfrac{1}{4}\sin(2\pi x)-\dfrac{1}{2}\widehat{h}_m, & |x|<1,\end{cases}\qquad h_2(x,0)=\begin{cases}1-\dfrac{1}{2}\widehat{h}_m, & |x|\ge 1,\\ 1+\dfrac{1}{4}\sin(2\pi x)-\dfrac{1}{2}\widehat{h}_m, & |x|<1,\end{cases}$$

$$h_m(x,0)\equiv\widehat{h}_m,\quad u_1(x,0)\equiv\widehat{u}_1,\quad u_2(x,0)\equiv\widehat{u}_2,\quad u_m(x,0)\equiv\frac{r\widehat{u}_1+\widehat{u}_2}{r+1},$$

with $\widehat{u}_1=0.4$ and $\widehat{u}_1=-0.4$. We take $B(x)\equiv-2$ and implement free boundary conditions on the computational domain $[-2,2]$. The initial setting for $h_m=0.2$ is shown in Figure 4.1. The simulations are run on the uniform grid with $\Delta x=1/200$ until time $t=0.5$.

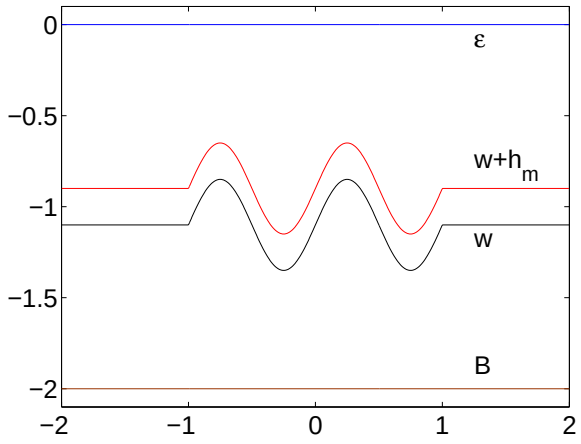


Figure 4.1: Example 1: The initial setting for the three-layer system with $\widehat{h}_m=0.2$.

We first compute the numerical solution of the two-layer system ($\widehat{h}_m=0$). The obtained results are presented in Figure 4.2. It is easy to check that in this case a large difference in initial velocities corresponds to the nonhyperbolic regime, which explains an oscillatory behavior of the computed solution. We then introduce a thin intermediate layer by taking $\widehat{h}_m=0.05$ and compute the corresponding numerical solution of the three-layer system. As one can see in Figure 4.3, the computed solution is still oscillatory, but the magnitude of oscillations is smaller than in the two-layer solution. When the initial thickness of the intermediate layer is increased to $\widehat{h}_m=0.1$, the oscillations are further reduced (see Figure 4.4). Finally, when we take $\widehat{h}_m=0.2$, the solution is practically non-oscillatory (see Figure 4.5). We therefore conclude that in this example, the studied three-layer approximation of the two-layer shallow water system leads to stabilization of the computed solution. However, one may argue that in the latter case of $\widehat{h}_m=0.2$ the "buffer" layer is not too thin and thus the three-layer model may not be considered as a minor modification of the original two-layer one.

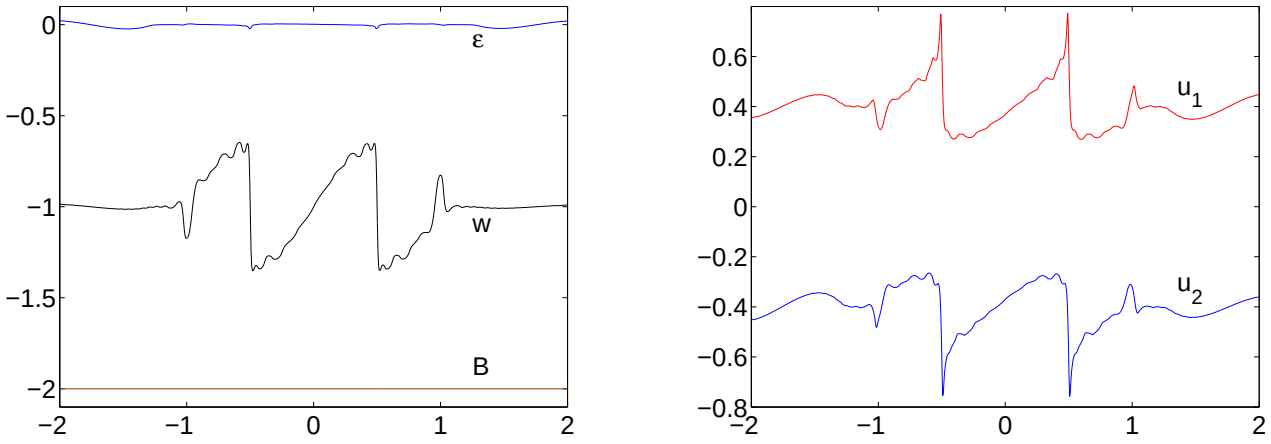


Figure 4.2: Example 1: Solution of the two-layer system ($\widehat{h}_m = 0$).

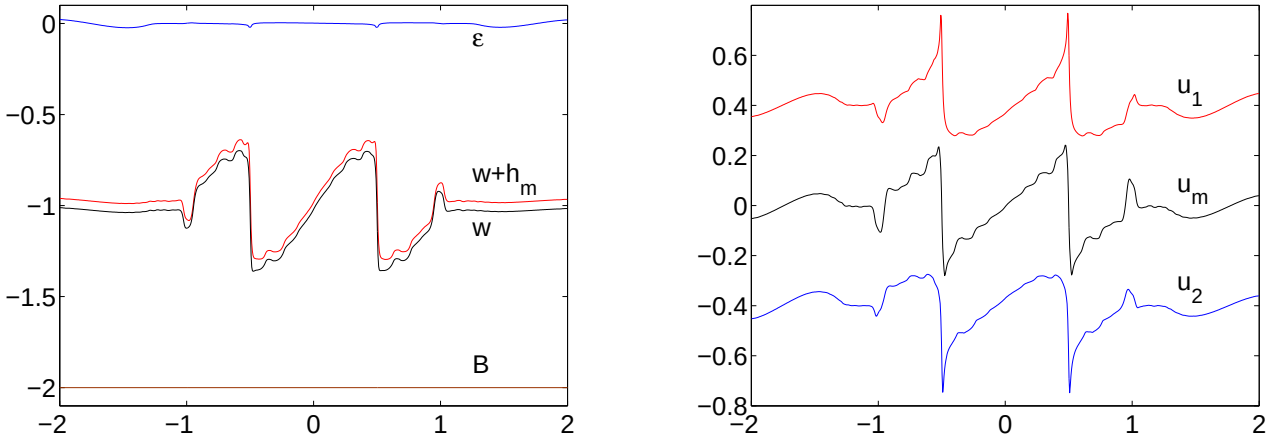


Figure 4.3: Example 1: Solution of the three-layer system with $\widehat{h}_m = 0.05$.

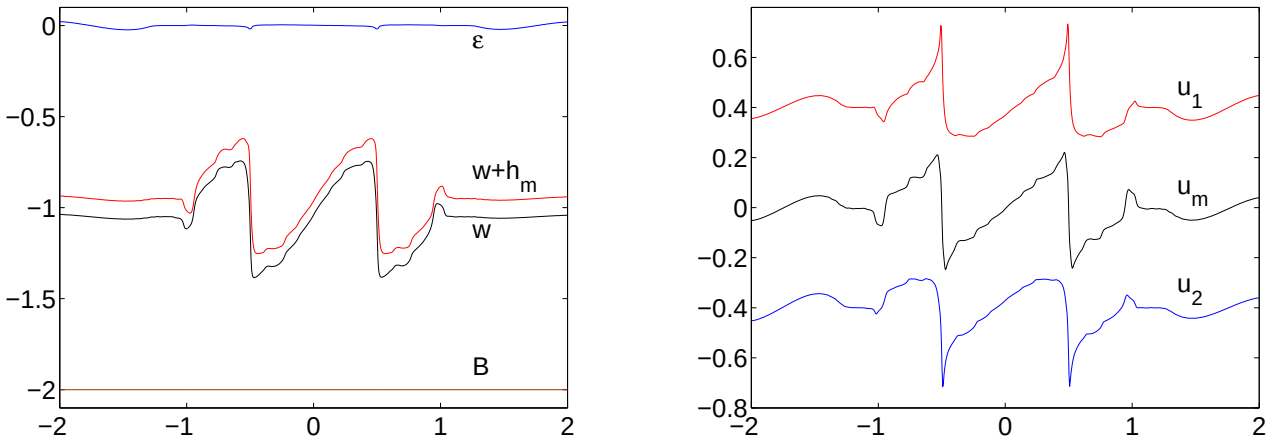


Figure 4.4: Example 1: Solution of the three-layer system with $\widehat{h}_m = 0.1$.

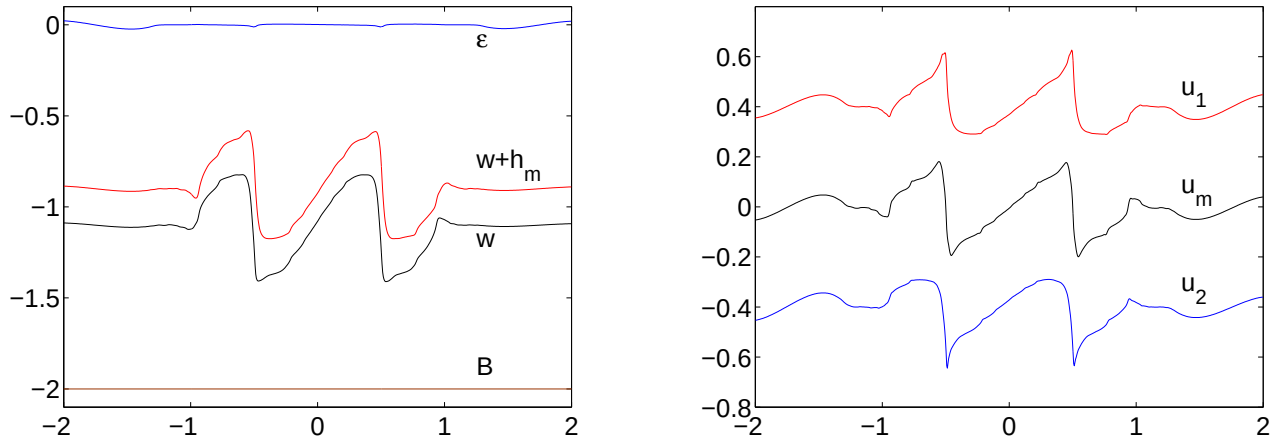


Figure 4.5: Example 1: Solution of the three-layer system with $\widehat{h}_m = 0.2$.

**Example 2.** We now consider the three-layer shallow water system (2.2) subject to the following initial data:

$$h_1(x,0) = 1.2 + 0.15\,(\tanh(5x) - \tanh(5x+10)) - 0.5\widehat{h}_m, \quad h_2(x,0) = -h_1(x,0) - B(x) - \widehat{h}_m,$$

$$h_m(x,0) \equiv \widehat{h}_m, \quad u_1(x,0) \equiv \widehat{u}_1, \quad u_2(x,0) \equiv \widehat{u}_2, \quad u_m(x,0) \equiv \frac{r\widehat{u}_1 + \widehat{u}_2}{r+1},$$

with $\widehat{u}_1 = 2.9$ and $\widehat{u}_1 = 2.1$. We take

$$B(x) = \begin{cases} -2, & |x| \geq 0.5, \\ -1.9 + 0.1\cos(2\pi x), & |x| < 0.5, \end{cases}$$

and implement free boundary conditions on the computational domain $[-3, 3]$. The initial setting for $h_m = 0.2$ is shown in Figure 4.6. Once again, we compute the numerical solution on the uniform grid with $\Delta x = 1/200$ and run the simulations until time $t = 0.5$.

As in Example 1, we first compute the numerical solution of the two-layer system ($\widehat{h}_m = 0$). The obtained results contain some oscillations in the internal wave as it can be seen in Figure 4.7. We then compute the numerical solutions of the corresponding three-layer systems with $\widehat{h}_m = 0.05$, 0.1 and 0.2. The situation is now completely opposite to the one observed in Example 1. When $\widehat{h}_m = 0.05$ the three-layer solution is clearly more oscillatory than the two-layer one (see Figures 4.8). Both $w$ and the velocities $u_1$, $u_m$ and $u_2$ develop oscillations. It is noticeable that the intermediate layer velocity $u_m$ does not stay in the range of the upper ($u_1$) and lower ($u_2$) layer velocities. When $\widehat{h}_m$ is further increased (see Figures 4.9 and 4.10), the solution becomes even more oscillatory. We thus conclude that in this example (unlike the previous one), the introduction of the "buffer" layer yield more severe instabilities and thus the three-layer approximation fails to achieve its goal of stabilizing the two-layer solution.

# 5 Discussion on the Hyperbolicity

As it has been mentioned above, the two-layer shallow water system (1.1) is only conditionally hyperbolic and in the nonhyperbolic regime, its solution typically develops instabilities. While in

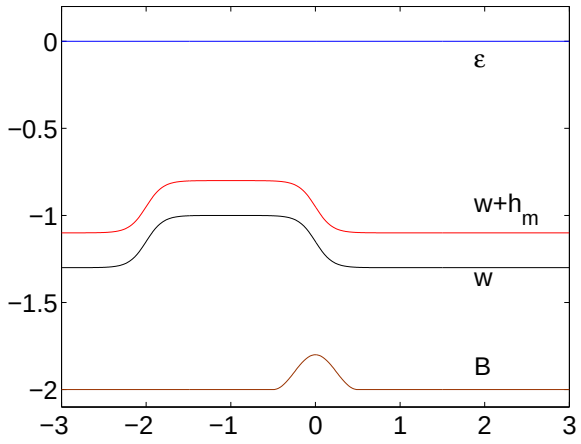


Figure 4.6: Example 2: The initial setting for the three-layer system with $\widehat{h}_m = 0.2$.

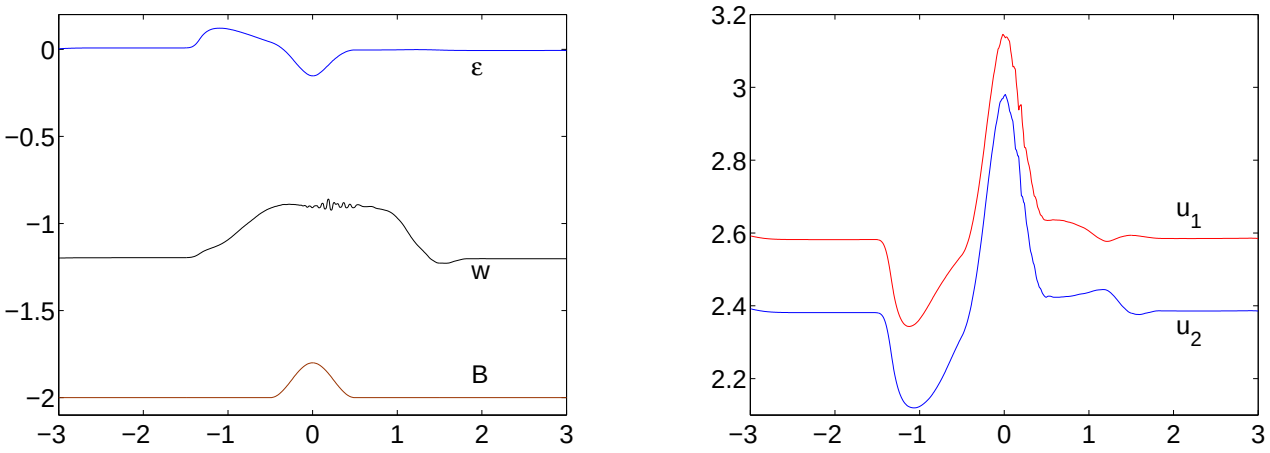


Figure 4.7: Example 2: Solution of the two-layer system ($\widehat{h}_m = 0$).

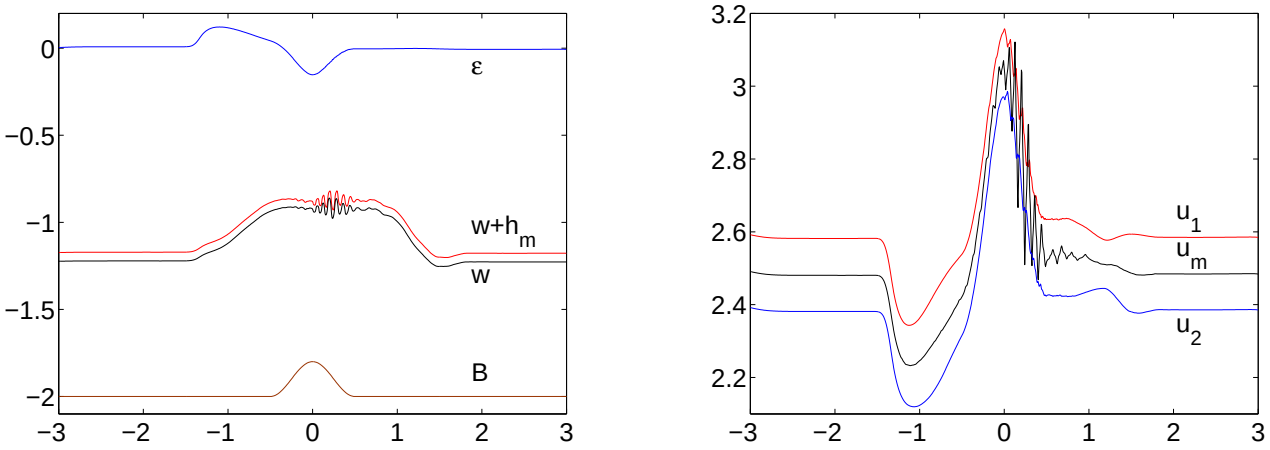


Figure 4.8: Example 2: Solution of the three-layer system with $\widehat{h}_m = 0.05$.

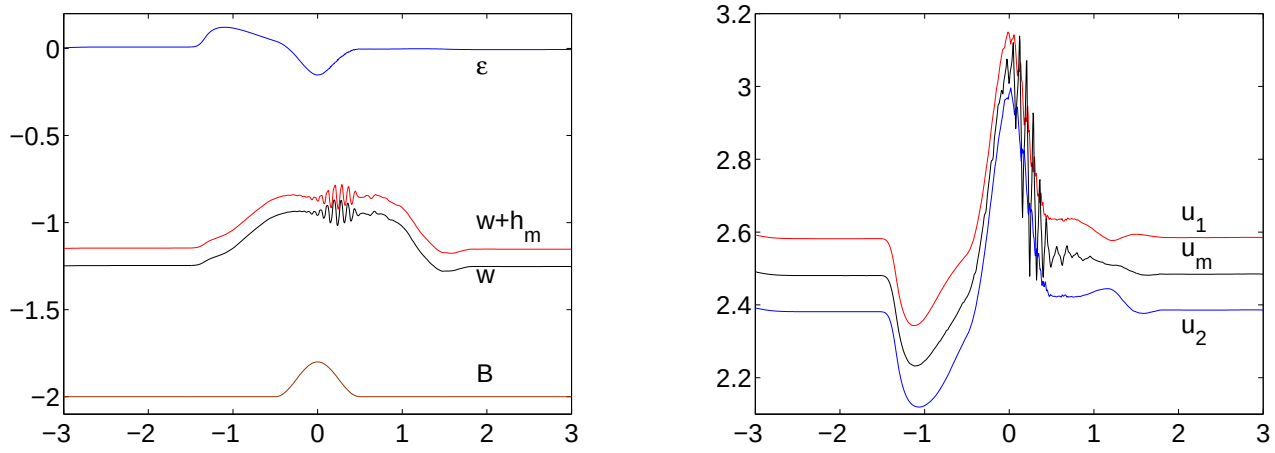


Figure 4.9: Example 2: Solution of the three-layer system with $\widehat{h}_m = 0.1$,

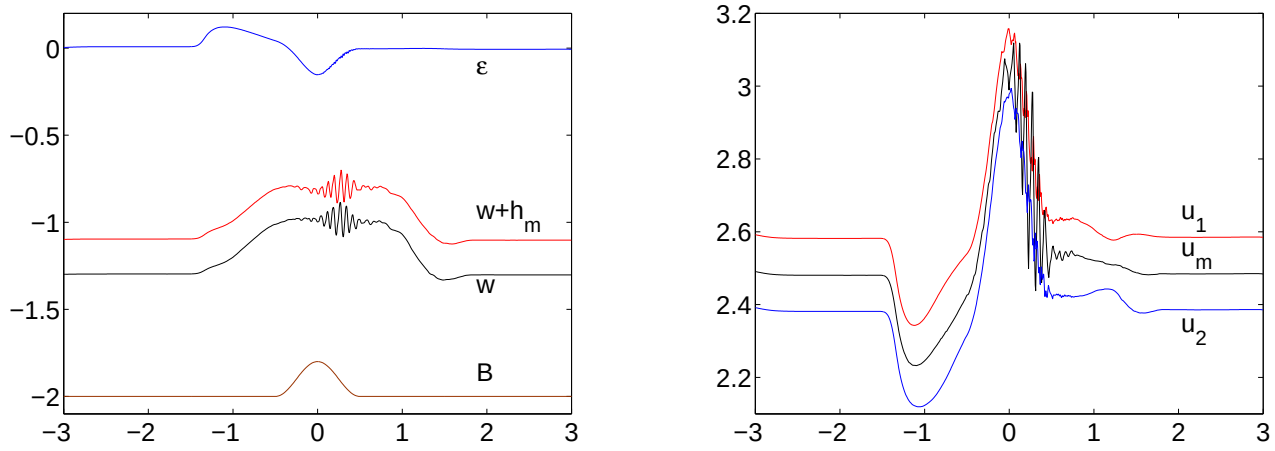


Figure 4.10: Example 2: Solution of the three-layer system with $\widehat{h}_m = 0.2$.

§4 we have demonstrated that in some situations the use of the three-layer approximation may improve stability properties of the system, in this section, we discuss and compare the hyperbolicity range of the three-layer system (2.1) and the original two-layer system (1.1).

We begin with examining the first-order approximation of the eigenvalues of the two-layer system (1.1) (see, e.g., [8, 25]), which is given by

$$\begin{aligned}
&\lambda_{1,2}(h_1,u_1,h_2,u_2) \approx U_m \pm \sqrt{g(h_1+h_2)},\\
&\lambda_{3,4}(h_1,u_1,h_2,u_2) \approx U_c \pm \sqrt{(1-r)g\frac{h_1h_2}{h_1+h_2}\left(1-\frac{(u_2-u_1)^2}{(1-r)g(h_1+h_2)}\right)},
\end{aligned} \tag{5.1}$$

where

$$U_m = \frac{h_1u_1+h_2u_2}{h_1+h_2}, \qquad U_c = \frac{h_1u_2+h_2u_1}{h_1+h_2}.$$

From (5.1), one expects that the two-layer shallow water system (1.1) is hyperbolic as long as

$$(u_2 - u_1)^2 < (1 - r)g(h_1 + h_2), \tag{5.2}$$

and thus the hyperbolicity condition for the two-layer shallow water system (1.1) depends on the relationship between $(u_2 - u_1)^2$ and $(1 - r)g(h_1 + h_2)$. To illustrate this relation we follow [6] and randomly choose the values of $h_1$, $h_2$, $u_1$ and $u_2$ and numerically check the hyperbolicity of each data set. The results are shown in Figure 5.1, where the values of $(1 - r)g(h_1 + h_2)$ are plotted against $(u_2 - u_1)^2$. In this figure, the hyperbolic region is marked using the blue points, while the nonhyperbolic one is specified using the red points. As one can see, the hyperbolic and nonhyperbolic regions are approximately separated by the straight line with the slope 1. This confirms the accuracy of the eigenvalue approximation used to obtain (5.2).

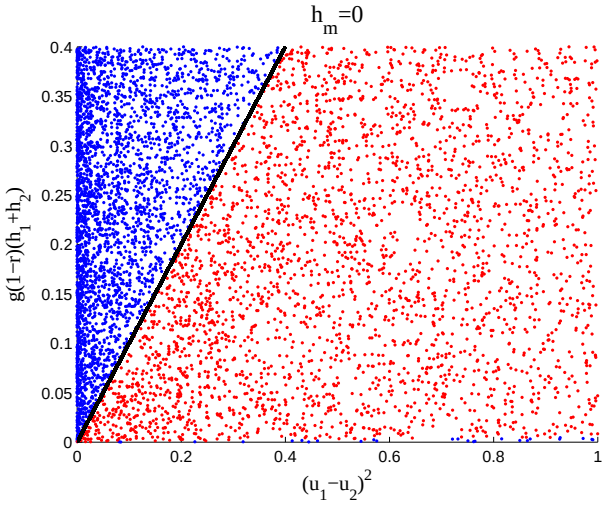


Figure 5.1: Hyperbolicity check for the two-layer system (1.1): The blue points represent the range of hyperbolicity.

We now perform a similar hyperbolicity study of the three-layer system (2.1), which for this purpose can be written in a the following quasi-linear form:

$$\begin{pmatrix} h_1 \\ q_1 \\ h_m \\ q_m \\ h_2 \\ q_2 \end{pmatrix}_t = \begin{pmatrix} 0 & 1 & 0 & 0 & 0 & 0 \\ gh_1 - u_1^2 & 2u_1 & gh_1 & 0 & gh_1 & 0 \\ 0 & 0 & 0 & 1 & 0 & 0 \\ \frac{2r}{1+r}gh_m & 0 & gh_m - u_m^2 & 2u_m & gh_m & 0 \\ 0 & 0 & 0 & 0 & 0 & 1 \\ grh_2 & 0 & \frac{1+r}{2}gh_2 & 0 & gh_2 - u_2^2 & 2u_2 \end{pmatrix} \begin{pmatrix} h_1 \\ q_1 \\ h_m \\ q_m \\ h_2 \\ q_2 \end{pmatrix}_x = -gB_x \begin{pmatrix} 0 \\ h_1 \\ 0 \\ h_m \\ 0 \\ h_2 \end{pmatrix}, \tag{5.3}$$

and numerically check whether all of the eigenvalues of the matrix on the left-hand side of (5.3) are real for the given set of data. Similarly to the two-layer case, we study the relationship between $(u_2 - u_1)^2$ and $(1 - r)gH$, where $H := h_1 + h_m + h_2$.

To this end, we first randomly select the total depth $H \in [0, 2]$, parameter $\alpha \in [0.3, 0.7]$, the velocities $u_1$ and $u_2$ such that $(0 \le |u_1 - u_2| \le 1)$ and set $h_2 := \alpha H - h_m/2$, $h_1 = (1-\alpha)H - h_m/2$.

We then let $h_m$ to vary from a very small value (0.01) to the larger values (0.05, 0.1 and 0.2) and to $1.9\min\big((1-\alpha)H,\alpha H\big)$, which is only 5% smaller than the largest theoretically possible value value of $h_m$. The obtained results are shown in Figures 5.2–5.4, where as before the hyperbolic regions are marked using the blue points and the nonhyperbolic ones are specified using the red points. Notice that since $H$ cannot be less than $h_m$, there is a (small) horizontal white strip at the bottom of each graph in Figures 5.2 and 5.3 (larger the $h_m$ larger the width of the white strip is).

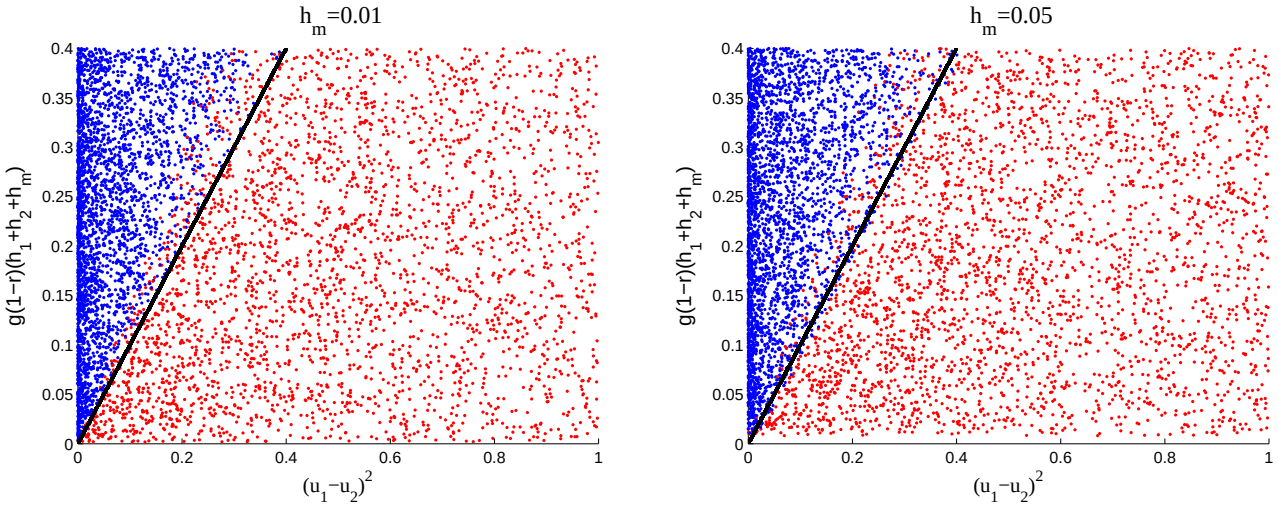


Figure 5.2: Hyperbolicity check for the three-layer system (2.1) with $h_m = 0.01$ (left) and $h_m = 0.05$ (right): The blue points represent the range of hyperbolicity.

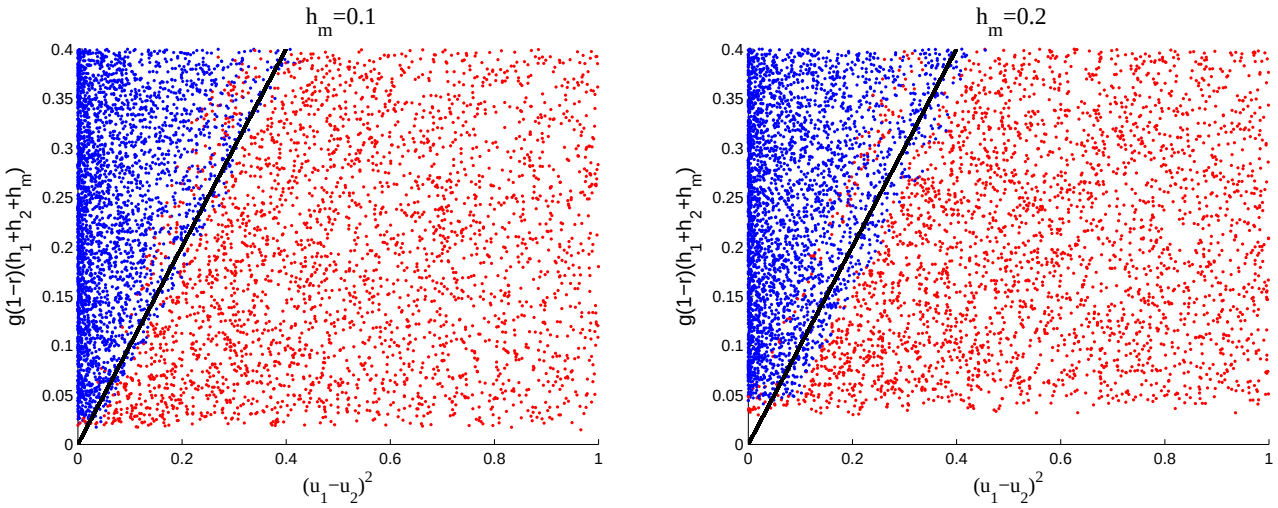


Figure 5.3: The same as in Figure 5.2 but with $h_m = 0.1$ (left) and $h_m = 0.2$ (right).

As one can see in Figures 5.2 and 5.3, in the three-layer case (unlike the two-layer one), there is no clear dividing line between the hyperbolic and nonhyperbolic regions for small and even intermediate values of $h_m$. However, one can observe that the hyperbolic region increases as $h_m$ increases. When $h_m$ reaches $h_m = 1.9\min\big((1-\alpha)H,\alpha H\big)$, the hyperbolic region for the three-layer

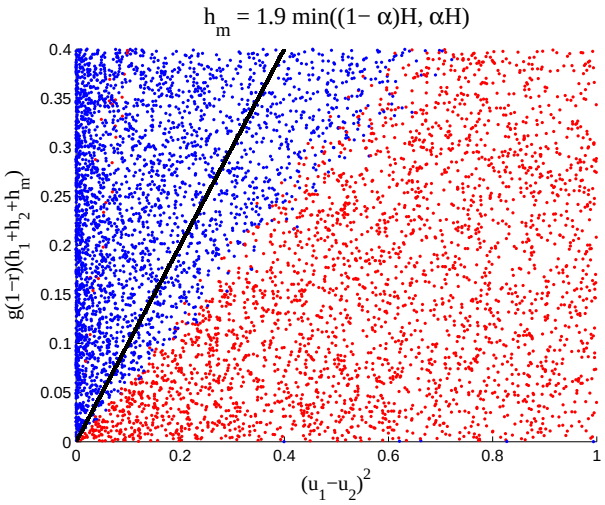


Figure 5.4: The same as in Figures 5.2 and 5.3 but with $h_m = 1.9 \min\left((1-\alpha)H, \alpha H\right)$.

system (see Figure 5.4) becomes about twice larger than the one for the corresponding two-layer system (see Figure 5.1). This experiment suggests that in order to significantly improve the hyperbolicity of the two-layer shallow water system, we need to introduce an unrealistically deep intermediate layer, which clearly cannot be considered as a "buffer" layer. Therefore, we arrive at the conclusion that even though adding the third layer may improve the stability properties of the two-layer shallow water system, a rigorous justification of the extent of the possible improvement is still an open problem we plan investigate in our future work.

**Acknowledgment:** The work of A. Chertock was supported in part by the NSF Grant DMS-1216974 and the ONR Grant N00014-12-1-0832. The work of A. Kurganov was supported in part by the NSF Grant DMS-1216957 and the ONR Grant N00014-12-1-0833. The work of Z. Qu was supported in part by the summer research stipend granted by the Mathematics Department at Tulane University. The work of T. Wu was supported in part by the NSF Grant DMS-1115718. A part of this research was conducted during the Summer of 2012, when the authors visited the Institute of Natural Sciences at the Shanghai Jiao Tong University, China. The authors would like to thank the faculty, staff and especially the Institute co-director Prof. Shi Jin for their support and hospitality.

# References

[1] R. ABGRALL AND S. KARNI, *Two-layer shallow water system: a relaxation approach*, SIAM J. Sci. Comput., 31 (2009), pp. 1603–1627.

[2] ——, *A comment on the computation of non-conservative products*, J. Comput. Phys., 229 (2010), pp. 2759–2763.

[3] E. AUDUSSE, *A multilayer Saint-Venant model: derivation and numerical validation*, Discrete Contin. Dyn. Syst. Ser. B, 5 (2005), pp. 189–214.

[4] E. AUDUSSE AND M.-O. BRISTEAU, *Finite-volume solvers for a multilayer Saint-Venant system*, Int. J. Appl. Math. Comput. Sci., 17 (2007), pp. 311–319.

[5] F. Bouchut and T. Morales de Luna, *An entropy satisfying scheme for two-layer shallow water equations with uncoupled treatment*, M2AN Math. Model. Numer. Anal., 42 (2008), pp. 683–698.

[6] M. Castro, J. Frings, S. Noelle, C. Pares, and G. Puppo, *Particle approximation of convection-diffusion equations*, IGPM report 314, RWTH Aachen University, 2010. Submitted to Proceedings of the 13th International Conference on Hyperbolic Problems (Peking, June 15-19, 2010).

[7] M. Castro, P. LeFloch, M. Muñoz-Ruiz, and C. Parés, *Why many theories of shock waves are necessary: convergence error in formally path-consistent schemes*, J. Comput. Phys., 227 (2008), pp. 8107–8129.

[8] M. Castro, J. Macías, and C. Parés, *A Q-scheme for a class of systems of coupled conservation laws with source term. Application to a two-layer 1-D shallow water system*, M2AN Math. Model. Numer. Anal., 35 (2001), pp. 107–127.

[9] M. Castro, A. Pardo, C. Parés, and E. Toro, *On some fast well-balanced first order solvers for nonconservative systems*, Math. Comp., 79 (2010), pp. 1427–1472.

[10] G. Dal Maso, P. Lefloch, and F. Murat, *Definition and weak stability of nonconservative products*, J. Math. Pures Appl. (9), 74 (1995), pp. 483–548.

[11] A. de Saint-Venant, *Thèorie du mouvement non-permanent des eaux, avec application aux crues des rivière at à l'introduction des marèes dans leur lit.*, C.R. Acad. Sci. Paris, 73 (1871), pp. 147–154.

[12] S. Gottlieb, C.-W. Shu, and E. Tadmor, *Strong stability-preserving high-order time discretization methods*, SIAM Rev., 43 (2001), pp. 89–112.

[13] A. Kurganov and D. Levy, *Central-upwind schemes for the saint-venant system*, M2AN Math. Model. Numer. Anal., 36 (2002), pp. 397–425.

[14] A. Kurganov and C.-T. Lin, *On the reduction of numerical dissipation in central-upwind schemes*, Commun. Comput. Phys., 2 (2007), pp. 141–163.

[15] A. Kurganov, S. Noelle, and G. Petrova, *Semi-discrete central-upwind scheme for hyperbolic conservation laws and Hamilton-Jacobi equations*, SIAM J. Sci. Comput., 23 (2001), pp. 707–740.

[16] A. Kurganov and G. Petrova, *A second-order well-balanced positivity preserving central-upwind scheme for the saint-venant system*, Commun. Math. Sci., 5 (2007), pp. 133–160.

[17] ——, *Central-upwind schemes for two-layer shallow equations*, SIAM J. Sci. Comput., 31 (2009), pp. 1742–1773.

[18] A. Kurganov and E. Tadmor, *New high resolution central schemes for nonlinear conservation laws and convection-diffusion equations*, J. Comput. Phys., 160 (2000), pp. 241–282.

[19] ——, *Solution of two-dimensional riemann problems for gas dynamics without riemann problem solvers*, Numer. Methods Partial Differential Equations, 18 (2002), pp. 584–608.

[20] K.-A. Lie and S. Noelle, *On the artificial compression method for second-order nonoscillatory central difference schemes for systems of conservation laws*, SIAM J. Sci. Comput., 24 (2003), pp. 1157–1174.

[21] M. Mignotte and D. Stefanescu, *On an estimation of polynomial roots by lagrange*, Tech. Rep. 025/2002, pp. 1–17, IRMA Strasbourg, `http://hal.archives-ouvertes.fr/hal-00129675/en/`, 2002.

[22] M. Muñoz-Ruiz and C. Parés, *On the convergence and well-balanced property of path-conservative numerical schemes for systems of balance laws*, J. Sci. Comput., 48 (2011), pp. 274–295.

[23] H. Nessyahu and E. Tadmor, *Nonoscillatory central differencing for hyperbolic conservation laws*, J. Comput. Phys., 87 (1990), pp. 408–463.

[24] C. Parés, *Numerical methods for nonconservative hyperbolic systems: a theoretical framework*, SIAM J. Numer. Anal., 44 (2006), pp. 300–321.

[25] J. Schijf and J. Schonfeld, *Theoretical considerations on the motion of salt and fresh water*, in Proc. of the Minn. Int. Hydraulics Conv., 1953, pp. 321–333.